Taylor & Francis
Taylor & Francis Group

Journal of Coordination Chemistry

ISSN: 0095-8972 (Print) 1029-0389 (Online) Journal homepage: http://www.tandfonline.com/loi/gcoo20

Volatile dimethylgold(III) complex with di-iso-butyldithiophosphinate ligand: synthesis, structure, and thermal behavior in condensed and gas phase

A.E. Turgambaeva, R.G. Parkhomenko, V.V. Krisyuk & I.K. Igumenov

To cite this article: A.E. Turgambaeva, R.G. Parkhomenko, V.V. Krisyuk & I.K. Igumenov (2015) Volatile dimethylgold(III) complex with di-iso-butyldithiophosphinate ligand: synthesis, structure, and thermal behavior in condensed and gas phase, Journal of Coordination Chemistry, 68:11, 1878-1889, DOI: 10.1080/00958972.2015.1032946

To link to this article: http://dx.doi.org/10.1080/00958972.2015.1032946

Accepted author version posted online: 27 Mar 2015.
Published online: 20 Apr 2015.

Submit your article to this journal

Article views: 32

View related articles

View Crossmark data

Full Terms & Conditions of access and use can be found at
http://www.tandfonline.com/action/journalInformation?journalCode=gcoo20

Download by: [Mizoram University] **Date:** 28 December 2015, At: 14:33

Journal of Coordination Chemistry, 2015
Vol. 68, No. 11, 1878–1889, http://dx.doi.org/10.1080/00958972.2015.1032946

Taylor & Francis
Taylor & Francis Group

Volatile dimethylgold(III) complex with di-*iso*-butyldithiophosphinate ligand: synthesis, structure, and thermal behavior in condensed and gas phase

A.E. TURGAMBAEVA*, R.G. PARKHOMENKO, V.V. KRISYUK and I.K. IGUMENOV

Nikolaev Insitute of Inorganic Chemistry SB RAS, Novosibirsk, Russia

(*Received 28 October 2014; accepted 11 March 2015*)

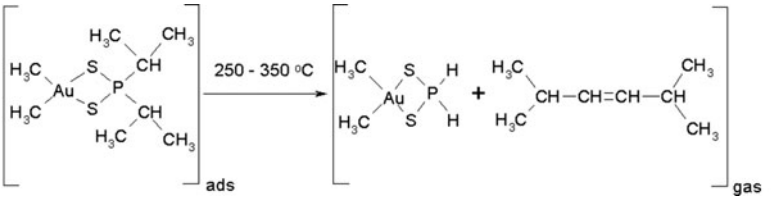

Synthesis and molecular structure of air stable, low-melting dimethylgold(III) complex with dithiophosphinate $(CH_3)_2AuS_2P^tBu^2$ (^{i}Bu=$CH_2CH(CH_3)_2$), its thermal properties, and the features as precursor for the metal–organic chemical vapor deposition of gold films are reported. Thermal behavior of the compound in the condensed and gas phase was studied by thermogravimetric analysis and mass spectrometry. Pathways of heterogeneous thermolysis of the compound to elemental gold are discussed. It was found that α-P–H elimination followed by coupling of two alkenyl groups from the coordinated ligand is one of the main thermolysis pathways in condensed and gas phase.

Keywords: Volatile dimethylgold(III) complexes; Thermolysis; Gold dialkyldithiophosphinate; Gold films deposition

Downloaded by [Mizoram University] at 14:33 28 December 2015

1. Introduction

Gold has been used in electrochemical applications, electronics, nanotechnology, in the areas of organic synthesis, catalysis, photophysics and photochemistry, biomedical applications, chemotherapy, etc. [1–11]. Gold forms a wide variety of organic derivatives [12, 13]. The chemistry of gold(III) complexes is far less developed than the corresponding gold(I) complexes. Gold(III) gives stable complexes with C, N, P, S, or O-donor ligands [14]. To manufacture gold thin film materials and nanoparticles on complex shape and non-planar surfaces, metal–organic chemical vapor deposition (MOCVD) is one of the most perspective techniques [15]. Conventional MOCVD is based on decomposition of the precursor's vapor on the heated substrate. Therefore, thermal properties of the metal–organic complex

*Corresponding author. Email: tae@niic.nsc.ru

© 2015 Taylor & Francis

Downloaded by [Mizoram University] at 14:33 28 December 2015

such as volatility (which is relatively high vapor pressure at modest temperatures or ability to pass into gas phase without decomposition) and stability in the condensed and gas phases are important parameters to be used as the precursor. Volatile gold(III) compounds investigated as gold CVD precursors mainly include dimethylgold(III) β-diketonates [16–18], carboxylates, salicylaldimines dialkyldithiophosphate, and diethyldithiocarbamate complexes [19–23]. In contrast to gold(I) compounds [24–26], above mentioned gold(III) compounds, with the exception of dimethylgold(III) salicylaldimines, do not require special synthesis and handling conditions. Dimethylgold(III) salicylaldimines are air-, moisture-, and light-sensitive compounds and have considerably less thermal stability and volatility.

Here we report on synthesis and molecular structure of Me_2AuL ($L = S_2P^iBu_2$, $Me = CH_3$, $^iBu = CH_2CH(CH_3)_2$), which represents complex of dimethylgold(III) with dialkyldithiophosphinate ligand, their thermal properties and the features as precursor for the MOCVD of gold films. Synthesis of air stable crystalline complex $Me_2AuS_2PMe_2$ (m.p. 48–50 °C) differing from Me_2AuL by the alkyl substituent in the ligand has been reported before, but data on the structure and thermal properties were not given [27]. Thermal behavior of the compound in the condensed and gas phase was studied by thermogravimetric analysis (TGA) and mass spectrometry (MS). Based on data on gaseous products composition, pathways of heterogeneous thermolysis of the compound to elemental gold are discussed. To test the compound as precursor for gold film deposition, it was subjected to low-pressure CVD with the *in situ* mass spectrometric analysis of the gas phase and to MOCVD at total pressure 10 Torr.

2. Experimental

2.1. *Synthesis*

Solution of $NaL{\cdot}3H_2O$ (Merck, purity > 98%) (0.12 g) in 20 mL of THF was added to solution of Me_2AuI complex (synthesized by the technique described by Zharkova *et al.* [28]) (0.2 g) in 10 mL of THF at a ratio of 1 : 1 for the reagents. The reaction mixture was stirred at room temperature for 1 h. The air-dried product was purified by column chromatography (SiO_2, hexane). Under ambient conditions, the complex represents transparent oily liquid (m.p. ~18 °C).

IR (cm^{-1}): 2959–2808 (–CH_3, C–H), 1463, 1396, 1368, 1219 (Au–CH_3), 1188, 1165, 1110, 1064, 839, 808 (Au–CH_3), 777 (P-S), 721 (P-C), 587 (AuC_2), 527. MS (EI, 70 eV): *m/z* (*I*, %) = 436 (3) $[M]^+$, 406 (86) $[AuL]^+$, 350 (77) $[HAuS_2PC_4H_9]^+$, 316 (100) $[AuS_2C_4H_8]^+$. Anal. Calcd for $C_{10}H_{24}AuPS_2$ (%): C, 27.5; H, 5.50; S, 14.7. Found: C, 27.4; H, 5.45; S, 14.3. Yield: 90%. ^{1}H NMR: δ 1.01 (s, 3H, Au–C$\underline{H_3}$), δ 1.16 (d, 6H, $J_{H\text{-}H}$ = 6.7 Hz, CH–(C$\underline{H_3}$)$_2$), δ 1.94 (q, 2H, $J_{H\text{-}H}$ = 6.2 Hz; $J_{P\text{–}H}$ = 10.7 Hz, P–C$\underline{H_2}$–CH), δ 2.36 (m, 1H, $J_{H\text{-}H}$ = 6.5 Hz, CH_2–C$\underline{H}$–$(CH_3)_2$).

2.2. *Physical measurements*

The TGA was performed at atmospheric pressure in a helium flow (30 mL min^{-1}) from 20 to 350 °C using a TG 209 F1 Iris® (NETZSCH) thermobalance and a standard open crucible. ^{1}H NMR spectra were recorded using a Bruker Avance 500 spectrometer (300 MHz, 25 °C); $CDCl_3$ was used as a solvent. The elemental analysis was performed using a

EuroEA3000, Eurovector. IR spectra were recorded from 400 to 4000 cm^{-1} on a Scimitar FTS2000 spectrometer using liquid film between KBr plates.

2.3. *X-ray crystallographic study*

The structure of the compound was solved by single-crystal X-ray diffraction analysis. Evaporating the solvent from hexane solution in a refrigerator afforded single crystals of the compound. Suitable single crystal was mounted on a Bruker Nonius X8 Apex 4 K CCD diffractometer fitted with graphite monochromated Mo-K_α radiation ($\lambda = 0.71073$ Å). The data were collected at 100 K by the standard technique [29]. Absorption corrections were made empirically using SADABS. The structure was solved using direct methods of the difference Fourier synthesis and were refined using the full-matrix least-squares method and the SHELXTL program set [30]. Positions of hydrogens were calculated geometrically and refined in the rigid body approximation (riding model). The crystallographic data are given in table 1.

2.4. *Mass spectrometric study*

MS was used to identify the compound, to evaluate its vaporization stability as well as to monitor the changes in the composition of the gas phase during the programed heating of the compound vapor.

Table 1. Crystal data and structure refinement for Me_2AuL.

Formula	$C_{10}H_{24}AuPS_2$
Formula weight	436.35
Temperature (K)	100(2)
Wavelength	0.71073
Crystal system	Monoclinic
Space group	$P2_1/c$
Unit cell dimensions	
a (Å)	$a = 15.0367(7)$
b (Å)	$b = 19.1518(8)$
c (Å)	$c = 11.1284(5)$
α (°)	90
β (°)	111.0180(10)
γ (°)	90
V (Å^3)	2991.5(2)
Z, calculated density (mg m^{-3})	8, 1.938
Absorption coefficient (mm^{-1})	10.190
F(0 0 0)	1680.0
Crystal size (mm)	0.35 × 0.26 × 0.15
θ Range for data collection	From 1.45 to 26.37
Limiting indices	$-18 \le h \le 18$, $-23 \le k \le 23$, $-13 \le l \le 13$
Reflections collected/unique (R_{int})	15854/4057 [R(int) = 0.0235]
Completeness to $\theta = 25{,}00°$ (%)	63.5
Absorption correction	Semi-empirical from equivalents
Maximum and minimum transmission	0.3102 and 0.1247
Refinement method	Full-matrix least squares on F^2
Data/restraints/parameters	4057/0/265
Goodness-of-fit on F^2	1.028
Final R indices [$I > 2\sigma(I)$]	$R_1 = 0.0196$, $wR_2 = 0.0449$
R indices (all data)	$R_1 = 0.0263$, $wR_2 = 0.0467$
Largest difference in peak and hole (eA^{-3})	1.895 and −0.791

Downloaded by [Mizoram University] at 14:33 28 December 2015

MS study was performed using a time-of-flight mass spectrometer (MSKh-6, USSR, mass range 3000 amu.) equipped with a special input system for investigating the volatile metal–organic compounds [31]. The ionization was performed by electrons with an energy of ca. 70 eV. Data collection and processing were performed using the National Instruments Corp. hardware and software. The following procedure was used. The compound *ca.* 1 mg was placed in a glass ampoule and was maintained at $T_e = 80$ °C in the evaporator under dynamic vacuum conditions. The vaporized compound passed into the reactor, which was heated from T_e to 400 °C with a rate of 5 min^{-1}. The reaction mixture entered the mass spectrometer ion source directly through the 0.2 mm effusive orifice of the reactor. To characterize the gas phase composition, full-range mass spectra were recorded every 2 min during the reactor heating.

Downloaded by [Mizoram University] at 14:33 28 December 2015

2.5. *Gold film deposition experiments and films characterization*

Deposition experiments were performed in a stagnant-flow, vertical cold-wall reactor at the following conditions: evaporator temperature $T_e = 80$ °C, deposition temperature $T_d = 250$ and 300 °C, total pressure – 10 Torr (1.33×10^3 Pa), argon was used as a carrier gas, the total flow rate 25 sccm. The Au films were deposited onto 8×8 mm^2 (100) oxidized silicon wafers subjected to a typical cleaning procedure. The deposition time was equal to 1 h. The films were submitted to X-ray photoelectron spectroscopy (XPS) using a SPECS (Germany) instrument. The photoelectron spectra were excited using monochromated Al Kα radiation ($h\nu = 1486.74$ eV) with the source power of 200 W and X-ray beam diameter of 6 mm. Analyses were performed after etching the external layer of the film with Ar^+ ions. The scanning electron microscopy (SEM) images of the films were recorded using a JEOL-JSM 6700 F scanning electron microscope. The thickness of the deposited films was measured using interference microscopy with a laser profilometer (Zigo 6300 New View).

3. Results and discussion

3.1. *Synthesis and identification*

The obtained compound represented colorless oily liquid at room temperature. The formulation was confirmed by elemental analysis and ^1H NMR being also consistent with the results of current mass spectrometric investigation. It was obtained in a high yield (about 90%) without use of special synthesis and handling conditions.

The molecular ion Me_2AuL of relative intensity 3% is observed in the mass spectrum confirming compound composition. The mass spectrum is dominated by the following fragmentary ions: $[AuL]^+$, $[HAuL\text{-}{}^iBu]^+$, $[AuL\text{-}H_2P{}^iBu]^+$ with the peak intensity being 86, 78, 100%, respectively ($L = S_2P{}^iBu_2$). The fragmentation of the molecular ion under electron impact results in formation of $[L]^+$ as well. The highest recorded mass in mass spectrum is due to molecular ion, indicating that the complex is monomeric in the gas phase.

3.2. *Crystal structure of Me_2AuL*

Me_2AuL crystallizes in the form of transparent colorless prismatic crystals at $T < 18$ °C. Crystal structure of compound consists of neutral molecules. Gold in the molecules has

slightly distorted square coordination constituted by two carbons of the methyl groups and two sulfurs of dithiophosphinate (figure 1). In the structure, there are two crystallographically independent molecules. Au–S distances are 2.4319–2.4507 Å, an average value of 2.4407 Å, that practically coincides with the length of Au–S bond (2.407 Å [32]) in $Me_2AuS_2CNEt_2$ having the same coordination. Chelating angles S–Au–S are less than 90° (82.68° and 82.65°). Mean bond length for Au–CH_3 is 2.057 Å, larger than that in dimethylgold(III) complexes with O- or N-donors [20, 33, 34]. However, in $Me_2AuS_2CNEt_2$, this distance is also equal to 2.057 Å [32]. This can be explained by strong *trans*-effect of the sulfurs in comparison with oxygen and nitrogen donors [35]. Angles C–Au–C are also less than 90° (table 2). The shortest distance between gold ions is 8.5826(4) Å. The molecules contact each other only by van der Waals interactions.

3.3. *Thermal behavior in the condensed phase*

As revealed by TGA (figure 2), the compound evaporates with partial decomposition with 80% mass loss from 70 to 150 °C. Amount of residue increased with increasing the heating rate: the reported compound has two losses of the weight with heating rate of 10 K min^{-1}. The first step of mass loss (~26%) observed from 115 to 190 °C may be attributed to the evolution of either two equivalents of C_4H_8 or one equivalent of C_8H_{16}. C_4H_8 can be isobutene formed due to β-P–H elimination, while C_8H_{16} can be 2,5-dimethyl-3-hexene formed due to α-P–H elimination with coupling of two alkyl groups. Both these processes should

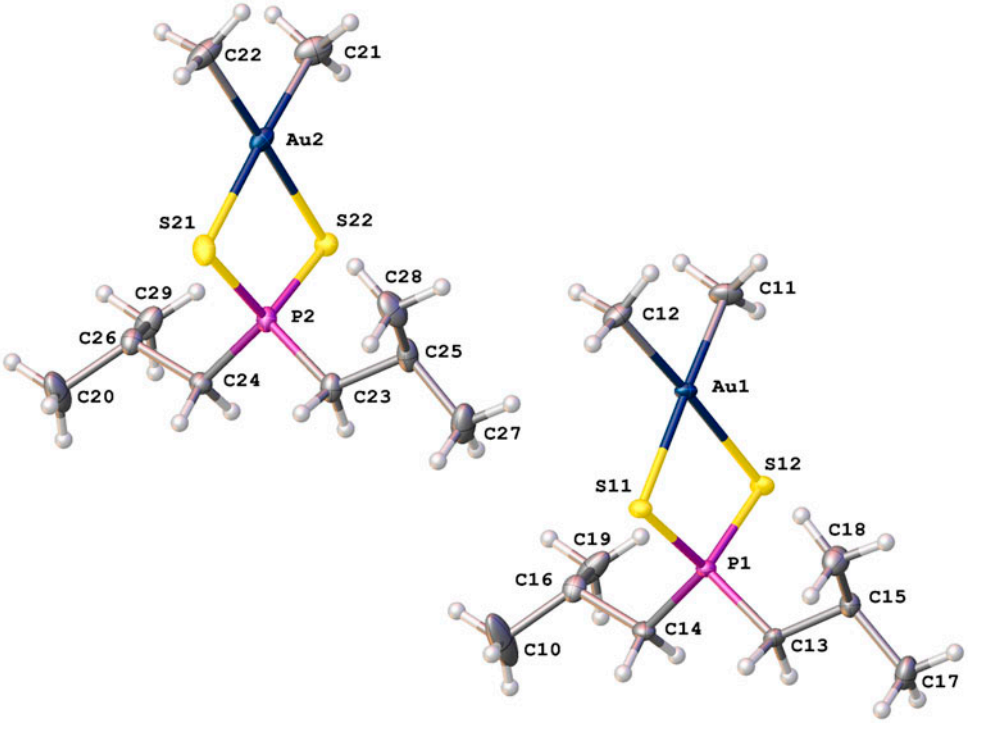

Figure 1. Molecular structure of Me_2AuL.

Downloaded by [Mizoram University] at 14:33 28 December 2015

Downloaded by [Mizoram University] at 14:33 28 December 2015

Table 2. Selected bond distances (Å) and angles (°).

Au1–S11	2.4333(10)
Au1–S12	2.4468(10)
Au1–C11	2.057(4)
Au1–C12	2.071(4)
Au2–S21	2.4507(11)
Au2–S22	2.4319(10)
Au2–C21	2.054(5)
Au2–C22	2.047(5)
S11–P1	2.0299(14)
S12–P1	2.0242(14)
S21–P2	2.0327(15)
S22–P2	2.0253(15)
S11–Au1–S12	82.68(3)
C11–Au1–S11	177.95(13)
C11–Au1–S12	95.32(14)
C11–Au1–C12	87.1(2)
C12–Au1–S11	94.93(13)
C12–Au1–S12	177.31(13)
S22–Au2–S21	82.65(4)
C21–Au2–S21	177.54(14)
C21–Au2–S22	94.94(14)
C22–Au2–S21	96.06(17)
C22–Au2–S22	178.28(16)
C22–Au2–C21	86.4(2)
P1–S11–Au1	85.99(5)
P1–S12–Au1	85.75(5)
P2–S21–Au2	85.72(5)
P2–S22–Au2	86.38(5)
S12–P1–S11	105.32(6)
S22–P2–S21	105.23(7)

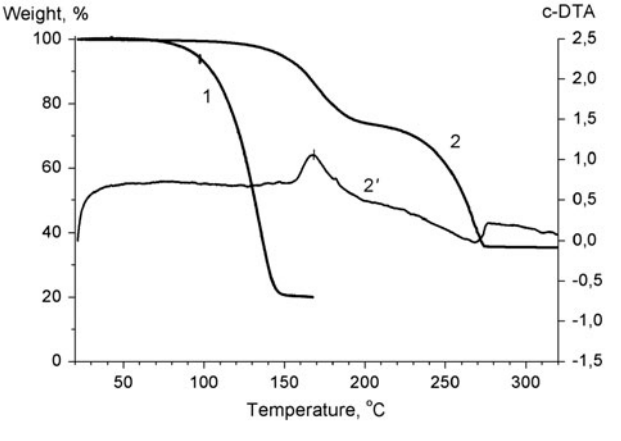

Figure 2. TGA results: 1, 2 – TG curves at heating rate 1 and 10 K min^{-1}, respectively, 2′ – DTA curve at heating rate 10 K min^{-1}.

result in the intermediate $Me_2AuS_2PH_2$. Smooth one step mass loss together with a single exothermic peak on the DTA curve indicates in favor of evolution of C_8H_{16}. This gaseous product formation is also confirmed by MS study of the heterogeneous thermolysis (occurrence of the molecular ion peak at *m/z* 112 and corresponding fragmentary ions). The second step of mass loss corresponds to evaporation of $Me_2AuS_2PH_2$ with decomposition from 190 to 270 °C giving the residue of 35% from the source compound. On the DTA curve, it is represented as an extended endothermic peak.

As far as vaporization stability is concerned, the complex withstood at least two cycles consisting of heating up to 80 °C and cooling in an evacuated evaporator (no change in the mass spectrum was observed).

3.4. *Heterogeneous thermolysis of Me_2AuL vapors*

The thermal decomposition was studied using an experimental setup consisting of an evaporator and a temperature-controlled cell (thermal reactor) built into the mass spectrometer, which allowed us to obtain temperature-resolved mass spectrum of the gas phase during compound vapor heating. The temperature dependences of the ion peak intensities were derived from the full-range mass spectra (figure 3). Fitting curves are result of three-point adjacent averaging smoothing of the experimental points. They are similar to classic kinetic concentration dependences and characterize the gas phase upon heterogeneous decomposition (due to the experimental conditions, all conversions occur on the hot walls of the

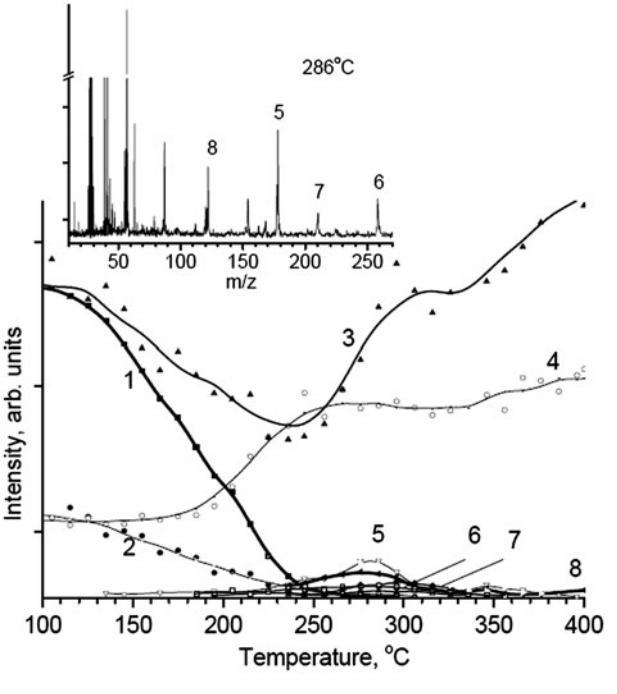

Figure 3. Temperature dependence of the gas phase composition for the decomposition of the complex reported (curves 1 and 2 refer to the entire precursor): 1 – $[AuL]^+$, 2 – $[L]^+$, 3 – $[C_3H_5]^+$, 4 – $[C_2H_4]^+$, 5 – ion with *m/z* 178, 6 – $[Me_2AuP]^+$, 7 – $[HL]^+$, 8 – ion with *m/z* 122.

Downloaded by [Mizoram University] at 14:33 28 December 2015

Downloaded by [Mizoram University] at 14:33 28 December 2015

reactor). The changes in the mass spectrum at different temperatures allowed us to reveal gaseous products formed in the thermolysis of the vaporized compound. It should be recalled that due to experimental conditions, decomposition takes place only on a heated surface following the monomolecular process. Upon reaching the decomposition onset temperature, the intensities of the peaks of gold-containing ions and of $[S_2P^iBu_2]^+$ originating from the entire complex exhibit a decrease, whereas the intensities of the ion peaks corresponding to the products demonstrate an increase. For the reported compound this temperature is ≥170 °C. Compared to the complexes with the same coordination core AuC_2S_2, thermal stability of the reported compound vapors is lower than those inherent for $Me_2AuS_2CNEt_2$ [21] and slightly higher than those for $Me_2AuS_2P(OMe)_2$ and $Me_2AuS_2P(OEt)_2$ [23], 210, 160, and 150 °C, respectively. The maximum decomposition is achieved at a temperature whereby the intensity of Au-containing peaks is close to the background value. This temperature is about 250 °C. Comparing the recorded mass spectra with the reference ones from NIST mass spectral library, we attributed the observed product peaks as follows: *m/z* 28 – molecular ion of ethylene and fragment ion having the maximal intensity in the mass spectrum of ethane, *m/z* 56 – molecular ion of isobutene (2-methylpropene) giving fragment ion of 100% intensity at *m/z* 41 (table 3). Apparently, peaks with *m/z* 210 and 154 relate to molecular ion of the protonated ligand HL and their fragment ion.[†] Molecular formula of the product producing under ionization a peak with *m/z* 178 may be $^iBu_2S_2$ (diisobutyldisulfide, ion mass/rel. abundance %: 178/23 122/11 57/100 41/27 29/20) or/and $^iBu_2SP(H)$ (diisobutylphosphine sulfide). Occurrence of two maxima at the curve of temperature dependence of ion peak intensity indicates the formation of two species. As to

Table 3. Major ion peaks in mass spectra and their assignments*.

m/z	Assignment
436	Me_2AuL – molecular ion M^+
406	AuL – fragment ion from M^+
350	$HAuS_2P\ ^iBu$ – fragment ion from M^+
316	$AuS_2C_4H_7$ – fragment ion from M^+
258	$[Me_2AuP]^+$ possibly fragment ion from $Me_2AuS_2PH_2$
210	$[HL]^+$ – protonated ligand
178	$[^iBu_2S_2]^+$ – dialkyldisulfide (231533) or/and $[SP(H)\ ^iBu_2]^+$ – dialkylphosphine sulfide
177	$[SP\ ^iBu_2]^+$ – fragment ion
154	$[H_2S_2P\ ^iBu]^+$ – fragment ion from the protonated ligand
122	$[Me_4P_2]^+$ – tetramethyldiphosphine and/or $[Et_2S_2]^+$ – diethyldisulfide (230585)
121	$[H\ ^iBuS_2]^+$ – fragment ion
112	Fragment ion
87	$[C_8H_{16}]^+$ – 2,5-dimethyl-3-hexene
63	$[SC_4H_7]^+$ – fragment ion
57	Fragment ion
56	$[C_4H_9]^+$ – fragment ion
41	$[C_4H_8]^+$
30	$[C_3H_5]^+$ – fragment ion
28	$[C_2H_6]^+$ – ethane (61308)
15	$[C_2H_4]^+$ – ethylene (18815) and fragment ion from ethane $[Me]^+$ – fragment ion

*NIST database number is indicated in the parentheses; L = $S_2P\ ^iBu_2$.

[†]Only isomeric di-n-butyldithiophosphinic acid was found in the database.

peak with *m/z* 258, we suppose that it has a formula $[Me_2AuP]^+$ and originates from $Me_2AuS_2PH_2$. This assumption is in accord with results of TGA of the compound in the condensed phase, indicating the formation of volatile product as a result of elimination of 2,5-dimethyl-3-hexene. The formation of protonated ligand is expected; it was already observed for other dimethylgold(III) complexes [36]. We have also recorded dialkyldisulfide as thermolysis product for dialkyldithiophosphate complexes [23], while formation of the product giving an ion at *m/z* 258 in mass spectrum is a surprising result. Based on obtained experimental data on gaseous products of the thermolysis, the pathways of decomposition of the compound to elemental gold can be hypothesized as given by Equations (1–3) (figure 4). During the pathway shown by Equation (1), the opening of chelate cycle of adsorbed molecule and protonation of the ligand result in evolution of the protonated ligand into gas phase, similar to decomposition of dimethylgold diethyldithiocarbamate [21]. Association/interaction of two surface-bound CH_3AuCH_2 moieties may result in the coupling product butane or the alkane and alkene disproportionation products. No mass spectrometric evidence of butane formation was found. Thus, ethane and ethylene and not the butane evolve into gas phase. As to evolution of the product giving a peak at *m/z* 178 in the mass spectrum, we propose that another gaseous product represented by peak at *m/z* 122 is produced during this decomposition pathway (Equation (2)). However, both fragment ions from the product with formula weight 178 and molecular ion from the product with formula weight 122 contribute to the intensity of this peak.

MS setup used to study thermolysis did not allow making *ex situ* analysis of solid products. Taking into account that it amounts to a low-pressure chemical vapor deposition reactor, samples of deposited films (solid products) have been obtained in cold wall reactor operating at 10 Torr. Compatibility of data obtained by these two techniques was shown [37]. The deposits consist of gold (73.3 and 91.8 at.% for deposition at 300 °C in argon and in hydrogen, respectively) with carbon-containing impurities. It should be noted that the films are free from sulfur, confirming our suggestions concerning the composition of the solid products of precursor thermolysis based on MS investigation. Deposition experiments showed that films obtained at $T \leq 300$ °C are thin and not continuous (figure 5), indicating low deposition rate at that temperature. That is again in accord with MS study of thermolysis. As given by Equation (3), the pathway with evolution of 2,5-dimethyl-3-hexene results in non-effective use of precursor during gold CVD at temperature lower than 350 °C owing

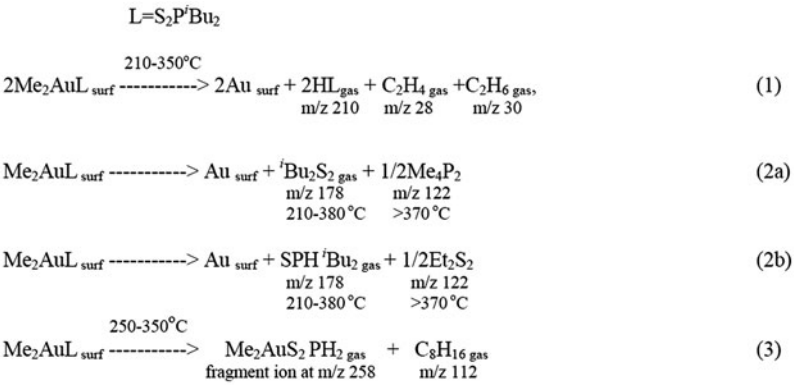

Figure 4. Me_2AuL thermolysis pathways.

Downloaded by [Mizoram University] at 14:33 28 December 2015

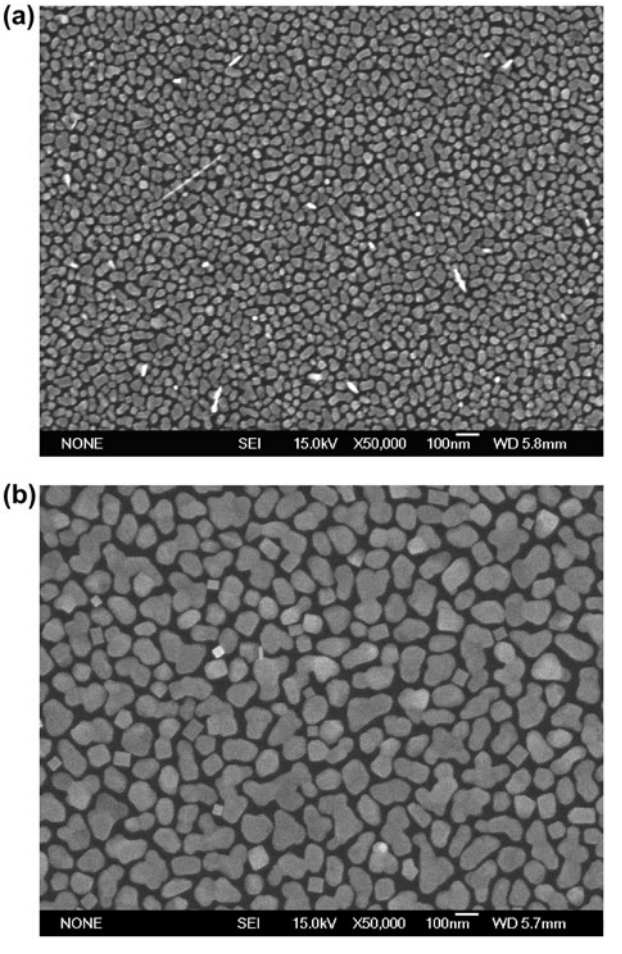

Figure 5. SEM images of gold films deposited from Me_2AuL: (a) Ar, 250 °C; (b) H_2, 300 °C.

to precursor not producing elemental gold. Thus, study of thermal behavior shows that the compound is not suitable for low temperature deposition of gold films. Probably, this can be overcome using deposition temperature higher than 350 °C.

4. Conclusion

Air stable low-melting organogold(III) complex Me_2AuL has been synthesized. The structure of the complex has been crystallographically characterized. Pathways of decomposition of the compound on heated surface to elemental gold have been proposed. It was found that α-P–H elimination followed by coupling of two alkenyl groups from the coordinated ligand is one of the main thermolysis pathways in condensed and gas phase. This can produce low yield of gold film in spite of satisfactory volatility and vaporization stability for the compound to be used in CVD techniques.

Downloaded by [Mizoram University] at 14:33 28 December 2015

Supplementary material

CCDC 887875 contains the supplementary crystallographic data for this paper. 15 These data can be obtained free of charge via http://www.ccdc.cam.ac.uk/conts/retrieving. html, or from the Cambridge Crystallographic Data Center, 12 Union Road, Cambridge CB2 1EZ, UK; Fax: (+44) 1223 336 033; or E-mail: deposit@ccdc.cam.ac.uk.

Acknowledgement

The authors are grateful to Mr S.V. Trubin (Nikolaev Institute of Inorganic Chemistry SB RAS) for XPS measurements.

Downloaded by [Mizoram University] at 14:33 28 December 2015

Disclosure statement

No potential conflict of interest was reported by the authors.

References

[1] M. Rudolph, A.S.K. Hashmi. *Chem. Soc. Rev.*, **41**, 2448 (2012).
[2] Z. Li, C. Brouwer, C. He. *Chem. Rev.*, **108**, 3239 (2008).
[3] M. Murdoch, G.I.N. Waterhouse, M.A. Nadeem, J.B. Metson, M.A. Keane, R.F. Howe, J. Llorca, H. Idriss. *Nat. Chem.*, **3**, 489 (2011).
[4] D.A. Giljohann, D.S. Seferos, W.L. Daniel, M.D. Massich, P.C. Patel, C.A. Mirkin. *Angew. Chem. Int. Ed.*, **49**, 3280 (2010).
[5] K. Saha, S.S. Agasti, C. Kim, X. Li, V.M. Rotello. *Chem. Rev.*, **112**, 2739 (2012).
[6] Y. Zhang, X. Cui, F. Shi, Y. Deng. *Chem. Rev.*, **112**, 2467 (2012).
[7] M. Stratakis, H. Garcia. *Chem. Rev.*, **112**, 4469 (2012).
[8] E.C. Dreaden, A.M. Alkilany, X. Huang, C.J. Murphy, M.A. El-Sayed. *Chem. Soc. Rev.*, **41**, 2740 (2012).
[9] P.T. Bishop, L.J. Ashfield, A. Berzins, A. Boardman, V. Buche, J. Cookson, R.J. Gordon, C. Salcianu, P.A. Sutton. *Gold Bulletin*, **43**, 181 (2010).
[10] A. Szentkuti, M. Bachmann, J.A. Garg, O. Blacque, K. Venkatesan. *Chem. Eur. J.*, **20**, 2585 (2014).
[11] Y.J. Lee, N.B. Schade, L. Sun, J.A. Fan, D.R. Bae, M.M. Mariscal, G. Lee, F. Capasso, S. Sacanna, V.N. Manoharan, G.R. Yi. *ACS Nano*, **7**, 11064 (2013).
[12] Patai's Chemistry of Functional Groups Series. *The Chemistry of Organogold Compounds*, Z. Rappoport, I. Marek, J.F. Liebman (Eds.), pp. 41–106, Wiley, Chichester, 2014. ISBN-13: 9781118438732.
[13] C. Corti, R. Holliday (Eds.), *Gold Science and Applications*, pp. 69–122, 217–230, CRC Press, Boca Raton, Chapters 5, 6, 10, 2009.
[14] M. Concepción Gimeno. In *Modern Supramolecular Gold Chemistry: Gold-Metal Interactions and Applications*, Antonio Laguna (Ed.), pp. 41–46, WILEY-VCH Verlag GmbH & Co. KGaA, Weinheim (2008), ISBN: 978-3-527-32029-5.
[15] Anthony C. Jones, Michael L. Hitchman (Eds.). *Chemical Vapour Deposition: Precursors, Processes and Applications*, pp. 207–254, Royal Society of Chemistry, Cambridge (2009).
[16] Y. Morishige, S. Kishida. *Appl. Phys. A*, **59**, 395 (1994).
[17] M. Okumura, S. Nakamura, S. Tsubota, T. Nakamura, M. Azuma, M. Haruta. *Catal. Lett.*, **51**, 53 (1998).
[18] P. Semyannikov, B. Moroz, S. Trubin, G. Zharkova, P. Pyryaev, M. Smirnov, V. Bukhtiyarov. *J. Struct. Chem.*, **47**, 458 (2006).
[19] A. Bessonov, N. Morozova, N. Gelfond, P. Semyannikov, S. Trubin, Y. Shevtsov, Y. Shubin, I. Igumenov. *Surf. Coat. Technol.*, **201**, 9099 (2007).
[20] A.A. Bessonov, N.B. Morozova, N.V. Gelfond, P.P. Semyannikov, I.A. Baidina, S.V. Trubin, Y.V. Shevtsov, I.K. Igumenov. *J. Organomet. Chem.*, **693**, 2572 (2008).
[21] A.E. Turgambaeva, G.I. Zharkova, P.P. Semyannikov, V.V. Krisyuk, T.P. Koretskaya, S.V. Trubin, B.M. Kuchumov, I.K. Igumenov. *Gold Bulletin*, **44**, 177 (2011).
[22] R.G. Parkhomenko, N.B. Morozova, G.I. Zharkova, Yu.V. Shubin, S.V. Trubin, V.V. Kriventsov, B.M. Kuchumov, T.P. Koretskaya, I.K. Igumenov. *Chem. Vap. Deposition*, **18**, 336 (2012).

[23] R.G. Parkhomenko, A.E. Turgambaeva, N.B. Morozova, S.V. Trubin, V.V. Krisyuk, I.K. Igumenov. *Chem. Vap. Deposition*, **19**, 38 (2013).
[24] P. Tran, P. Doppelt. *J. Electrochem. Soc.*, **154**, D520 (2007).
[25] J. Messelhäuser, E.B. Flint, H. Suhr. *Appl. Surf. Sci.*, **54**, 64 (1992).
[26] A. Grodzicki, I. Łakomska, P. Piszczek, I. Szymańska, E. Szłyk. *Coord. Chem. Rev.*, **249**, 2232 (2005).
[27] H.W. Chen, C. Paparizos, J.P. Fackler Jr. *Inorg. Chim. Acta*, **96**, 137 (1985).
[28] G. Zharkova, I. Igumenov, S. Zemskov. *Koord. Khim.*, **6**, 720 (1980) (in Russian).
[29] Bruker AXS Inc. *APEX2 (Version 1.08), SAINT (Version 7.03), and SADABS (Version 2.11), Bruker Advanced X-ray Solutions*, Bruker Advanced X-ray Solutions, Madison, WI. (2004).
[30] G.M. Sheldrick. *Acta Crystallogr. A*, **64**, 112 (2008).
[31] A.E. Turgambaeva, V.V. Krisyuk, P.A. Stabnikov, I.K. Igumenov. *J. Organomet. Chem.*, **692**, 5001 (2007).
[32] G.I. Zharkova, I.A. Baidina, I.K. Igumenov. *J. Struct. Chem.*, **48**, 108 (2007).
[33] A.A. Bessonov, I.A. Baidina, N.B. Morozova, P.P. Semyannikov, S.V. Trubin, N.V. Gelfond, I.K. Igumenov. *J. Struct. Chem.*, **48** 282 (2007).
[34] A.A. Bessonov, I.A. Baidina, N.B. Morozova, N.V. Kuratieva, N.V. Gelfond, I.K. Igumenov. *J. Struct. Chem.*, **49** 64 (2008).
[35] J.D. Atwood. *Inorganic and Organometallic Reaction Mechanisms*, 2nd Edn, VCH, Weinheim (1997).
[36] P.P. Semyannikov, V.M. Grankin, I.K. Igumenov, G.I. Zharkova. *J. Phys. IV*, **5**, 213–220 (1995).
[37] F. Senocq, A. Turgambaeva, N. Prud'homme, U. Patil, V.V. Krisyuk, D. Samélor, A. Gleizes, C. Vahlas. *Surf. Coat. Technol.*, **201**, 9131 (2007).

Downloaded by [Mizoram University] at 14:33 28 December 2015